Chapter 7

Luminescent Zeolites

Hui Lin and Minoru Fujii

Additional information is available at the end of the chapter

http://dx.doi.org/10.5772/63805

Abstract

Compared with the intensive fundamental research and practical application development of zeolites in the fields of photocatalysis, separation, ion exchange, and antimicrobial, research on the luminescence from optically functionalized zeolites is still at a juvenile stage. So far, plenty of important potential applications based on luminescent zeolites, such as light harvesting, phosphors, optical encoding/recording, micro-lasers, chemical sensors, and bio-imaging, have been demonstrated. What's more, it has been shown that the porous crystalline nature of zeolites makes them an excellent matrix for investigating the fundamental physics of the sub-nm-scale luminescent metal clusters, which is still not sufficiently clear till now. Due to its significance, luminescent zeolites functionalized by luminescence-active guest species in various types including organic dye molecules, rare earth (RE) ions, bismuth ions, and d^{10} metal ions are reviewed in this chapter, dedicating to presenting some representative work on luminescent zeolites during the past few decades, from materials design, preparation, to application demonstrations, in hope to boost more research interest and strength in this community.

To date, optically activated luminescent zeolites are mainly focused on several types of aluminosilicate zeolites with the dimension of pores or channels in the scale of about 0.3–1.5 nm, such as the FAU-type, the LTL-type, the LTA-type, the ZSM-5-type, and the SOD-type zeolites. Here, in this chapter, the zeolites mainly refer to these nanoporous zeolites functionalized by luminescent centers.

Keywords: luminescence, zeolites, rare earth ions, bismuth ions, noble and coinage metal clusters

1. Introduction

In Section 1, luminescence of zeolites functionalized by organic dye molecules and quantum dots incorporated within the cavities is reviewed. The strong capacity of incorporating and confining organic dye molecules and quantum dots into zeolites' cavities is enabled by the

large inner surface area, the exchangeable extra-framework cations, the built-in static electrical field between the extra-framework cations and the framework oxygen, and the well-confined periodically distributed cavities. Previous work on organic dye molecules or quantum dots containing zeolites with designed alignment of the guest dye molecules and sometimes the host zeolite micro-/nanocrystals is briefly introduced. Since most of these important work has been well summarized in some previous book chapters, reviews, or feature articles (Gion Calzaferri, *Top Catal*, 2010, 53:130–140; Gion Calzaferri, *Chapter 7* in *Photofunctional zeolites: synthesis, characterization, photocatalysis reactions, light harvesting*; & Calzaferri, *Langmuir*, 2012, 28:6216–6231; Gion Calzaferri, *Advances in Photochemistry*, 2002, 27:1–50; Thomas Bein, *Chapter 18* in *Introduction to Zeolite Molecular Sieves*, 3rd Edition, 2007), here we generally review some typical methods for processing the dye molecules containing zeolites and introduce some new achievements in this area within the recent years.

The extra-framework cations of zeolites such as Na^+, K^+, and Ca^{2+} are not as stable as the framework Si^{4+} and Al^{3+} and are exchangeable to other cations, for instance, the usage of zeolite 4A as water softener via the $Na^+ \rightarrow Ca^{2+}$ or Mg^{2+} exchange. The extra-framework cations can also be replaced by optically active centers such as rare earth (RE) ions, the transition metal (TM) ions, and some luminescence-active main group elements ions, for instance, bismuth (Bi) ions, etc. The porous crystalline nature of zeolites benefits the homogeneous dispersion of luminescence-active centers in the zeolite matrices. To present efficient luminescence from the RE ion- and Bi ion-exchanged zeolites, relieving or eliminating the influence of the hydrated water molecules is a prerequisite. In Section 2, recent achievements on the visible and NIR emission from the rare earth (RE) ion- and bismuth (Bi) ion-exchanged zeolites and their potential optical and photonics applications are reviewed.

d^{10} ion-exchanged zeolites, especially Ag^+ ion-exchanged zeolites, show excellent photocatalysis capacity. Comprehensive work on summarizing the photocatalysis properties of transition metal ion-exchanged zeolites has been conducted in a previous book "Photofunctional Zeolites: Synthesis, Characterization, Photocatalytic Reactions, and Light Harvesting." In Section 3, we mainly focus on the luminescence properties of these materials, aiming for potential optical and photonics applications. Due to the closed-shell electronic structure, usually there exist weak metallophilic interactions between the d^{10} ions, which exhibit many intriguing luminescence phenomena. Amazingly, the capability of adsorption/desorption of small polar molecules of the aluminosilicate nanoporous zeolites can have strong influence on the coordination of the extra-framework d^{10} ions and the metallophilic interaction between the adjacent d^{10} ions; in result reversible emission variation from the d^{10} ion-exchanged zeolites has been observed.

1.1. Incorporating organic dye molecules into zeolites' cavities

Dye molecules incorporated within the cavities of zeolites are representative guest-host materials which have significance to both fundamental research and technical applications. The distinct feature of zeolite matrices is their nature-born, spatially perfectly confined cages and channels enabled by its porous crystalline structure, which makes them superior to porous glasses or dense crystalline matrices. Dye molecules are often encapsulated within zeolites'

cavities via physisorption, self-assembly, ion exchange, crystallization inclusion, or direct synthesis in the cages or channels of zeolites (also called the ship-in-a-bottle method). The most frequently adopted zeolite matrices for organic dye molecules are those with strictly parallel one-dimensional (1D) channels, such as the LTL-type (short for L-type) and AFI-type zeolites, which can help simplify the investigation on the energy transfer process due to the strong 1D confinement of the dye molecules. By choosing proper organic dye molecules and zeolite matrix guest-host pairs, emission quenching due to the aggregation of dye molecules can be prevented by spatially confining the dye molecules at the monomer scale. Meantime, this features the high quantum yield emission by high concentration loading of organic dye molecules without aggregation-induced quenching. Anisotropic energy transfer among organic dye molecule guests and polarized emission parallel/perpendicular to the *c*-axis is possible to achieve within the dye molecules/1D-channel zeolites guest-host systems by proper spatial confinement of the dye molecules [1]. So far, various kinds of neutral, cationic organic dye molecules and their combination have been incorporated into the cavities of zeolites, including some dyes for laser generation [2]. To achieve patterned incorporation of the dye molecules into the orientation of well-aligned 1D-channel zeolite monolayers or arrays, sometimes micro-contact printing (mCP), which is usually used for fabricating or transferring the *c*-axis-oriented L-type or AFI-type zeolite monolayers or arrays, has been conducted [3].

Synthesis of *c*-axis-oriented 1D-channel zeolite monolayers or arrays with the channels open at the off-substrate ends and ready to load dye molecules has been of particular interest and intensively investigated [4]. To seal the entrance(s) to the 1D channels in case of dye molecule leakage after loading, stuffing at the end(s) of the 1D channels with molecules (phthalocyanine, for instance) serving as stopcock or surface coating is often performed [5]. In some cases, the stopcock molecules can also act as linkages so that they assemble the dye molecules containing 1D-channel zeolite micro-/nano-crystals end to end into chains.

1.2. Aligning the orientation of the 1D-channel zeolite micro-/nanocrystals in favor of photonics applications

Besides the controllable assembly of the organic dye molecules in the parallel 1D channels, orienting the micro-/nano-zeolite matrix grains to obtain well-aligned arrays or thin films is also highly expected to facilitate certain optical or photonic applications. Chemical modification [6], seeding-epitaxial growth [4], external magnetic field application [7], and micro-contact imprinting [8] have been utilized to align the zeolite micro-/nanocrystals along the 1D channel direction.

Obtaining zeolite micro-/nano-crystals monolayer via chemical interactions such as covalent linkages, ionic bonding, and hydrogen bonding has been summarized by Yoon [6]. Here we mainly introduce the orientation alignment via seeding-epitaxial growth and via external magnetic field assistance.

A typical process to obtain 1D-channel zeolite thin films with well-aligned grains by first loading a seeding layer on the substrate followed by the further epitaxial growth has been described as follows by Xue et al. [4]: first by surface modification of the quartz slice substrate using cation polymer, for example, poly(diallyldimethylammonium chloride) (PDDA), to get

a positively charged substrate surface as template for the zeolite seed crystals; then seeds loading via immersing the substrate horizontally in the seed crystals suspension, followed by rinsing and drying to get the seeds slice; growth of the *c*-axis-oriented AFI film by a further hydrothermal crystallization in the autoclave; organic template (PDDA) removal by calcinations; and finally dye molecules loading by adding the calcined *c*-axis-oriented AFI thin film in an azo dye molecule (DPPA) solution. This azo dye molecule containing *c*-axis-oriented AFI zeolite film shows ability for detecting heavy metal ions by monitoring the optical absorption variation, particularly efficient for the detection of Zn^{2+} ions.

Cucinotta et al. depicted a simple experimental layout for aligning the orientation of the zeolite L micro-cylinders via applying external magnetic field [9]. After dye molecule loading, monodisperse Fe_3O_4 nanoparticles prepared by chemical co-precipitation were coated on the surface of zeolite L microcrystals via natural assembly without any surface modification. The attached Fe_3O_4 nanoparticles can assist the alignment and the orientation of the zeolite L microcrystals.

Amazingly, alignment and the orientation of organic dye molecules incorporated into zeolite L microcrystals decorated by the Fe_3O_4 nanoparticles via external magnetic field can be achieved in aqueous solution, on solid substrates, and even in polymer matrices. The most interesting point may be that anisotropy in the optical absorption and emission spectra was observed and assigned to the fine spatial alignment of both the hexagonal zeolite L microcrystal matrices and the organic dye molecules within the matrices' 1D channels.

1.3. Featured luminescence from the dye molecules incorporated into zeolites

The most intensively conducted work on the luminescence properties of organic dye molecules incorporated into 1D channel zeolites is regarding the design and fulfillment of the efficient energy transfer from the donors to acceptor dyes via the Förster resonant energy transfer (FRET), typically aiming for artificial photosynthesis. An extreme fast non-radiative energy transfer from the donor to the acceptor (emitter) is required in case of energy loss via other pathways [10].

It is interesting that some organic dyes, hostasol red (HR), for instance, show efficient luminescence in aprotic solvents but becomes inefficient when it's incorporated into zeolite L's channels. By partial or complete exchanging the extra-framework K^+ ions with imidazolium cation, the emission quantum yield of the hostasol red (HR) dyes containing zeolite L can be enhanced to a large extent by reducing the proton activity of the extra-framework cations in water molecules environment [11]. Meantime, the high-emission quantum yield can be together ensured by locating the HR dyes in the middle of the 1D channels and in the environment of perylene dye serving as the antenna donor, in which condition a highly efficient donor-acceptor system can be formed.

1.4. Quantum dots (clusters) embedded in zeolite matrices

Due to the tiny sizes of the nanoporous zeolites' cavities (0.3–1.5 nm), the sizes of the semiconductor nanospecies confined within the zeolites' cavities are smaller than typical semiconductor quantum dots and they can be at the scale which consists of several "molecules" [12]. At this scale, the tiny semiconductor crystals are sometimes called quantum clusters. Zeolite matrices have the advantages of excellent size confinement and periodical spacing between the quantum dots. Owing to the size well-defined cages and channels, zeolites have also been demonstrated for screening out the semiconductor dots or clusters with narrow size distribution.

1.5. Possible future work

At present, the applied magnetic field for aligning the orientation of zeolite microcrystals in the recent reports is very high (1 T). Actually, even for the paramagnetic materials, Al_2O_3, or $Ca_5(PO_4)_3F$, for instance, under such strong magnetic field, aligning grains along the *c*-axis can be also be achieved [13, 14]. Efforts may be deserved on providing other novel structures or architectures or decorating methods which can reduce the applied magnetic field to facilitate the orientation alignment with moderate magnetic field.

2. Rare earth (RE) ion- and bismuth (Bi) ion-exchanged nanoporous zeolites and their derivatives

2.1. Factors influencing the luminescence quantum efficiency and possible solutions

2.1.1. Phonon energy of zeolites' frameworks

The framework of aluminosilicate zeolites consists of $[SiO_4]^{4-}$ and $[AlO_4]^{5-}$ tetrahedrons sharing the O^{2-} corners; the lattice vibration energy of the (dehydrated) zeolite framework itself is suitable to serve as a host material for luminescence.

2.1.2. Hydrate water molecules

As mentioned above, for these zeolites with the aluminosilicate composition, to keep charge neutral, cations such as Na^+, K^+, and Ca^{2+} are located in the channels and cages and are coordinated by the framework oxygen. The electric field existing between the extra-framework cations and the framework oxygen has strong attraction for small polar molecules. As a result, water molecules are easily adsorbed in this type of zeolites such as the LTA and FAU types, usually with the H atoms bonded to the framework oxygen or with the O atoms coordinated to the extra-framework cations.

Hydrated water molecules are the most influencing factor on the emission efficiency of the optically functionalized luminescent zeolites. On the one hand, due to the high vibrational energy (maximal ~3600–3700 cm^{-1}), hydrated water molecules are generally detrimental to the

emission efficiency of the RE and Bi ion-exchanged zeolites. To achieve efficient luminescence from these types of optically activated zeolites and its derivatives, dehydration and then preventing rehydration via stuffing the entrance for water molecules [15], or filling the cavities with molecules or radicals of low vibrational energy [16], are two often adopted methods.

On the other hand, interestingly, it has been demonstrated in our recent work that the hydrated water molecules are essential to the strong yellow-green emission from the Ag^+ ion-exchanged LTA zeolites, which can be attributed to the coordination to the Ag^+ ions that ensures an efficient ligand to metal charge transfer (LMCT) process. This part will be discussed with more details in Section 3.

2.2. Down-conversion near-infrared (NIR) emission from Nd^{3+} ion-exchanged zeolite Y

Nd^{3+} is a representative RE ion as the NIR luminescence-active center in various matrices (one peak at ~1.06 μm and the other at ~1.35 μm), for instance, the Nd^{3+}-doped phosphate glass or the Nd^{3+}-doped yttrium aluminum garnet (usually denoted as Nd^{3+}:YAG) single crystal for solid-state laser generation.

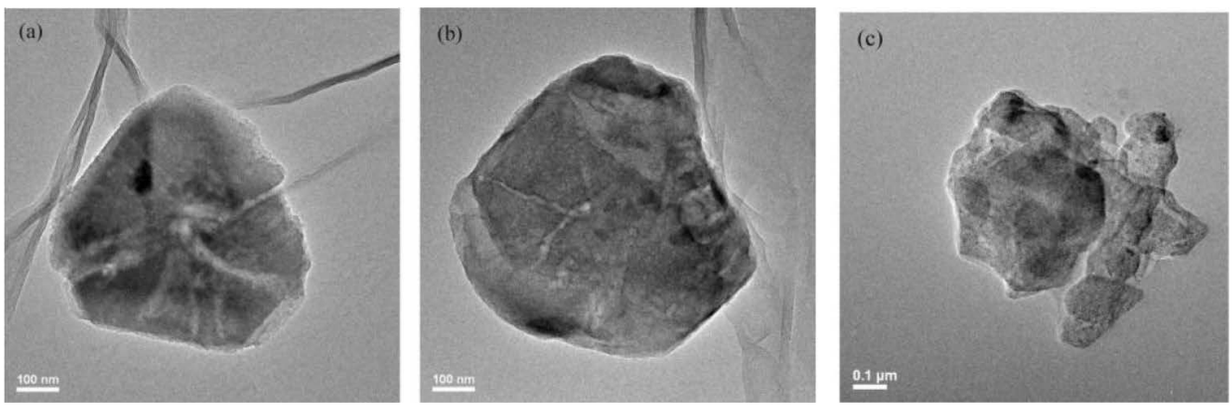

Figure 1. TEM morphology of pure zeolite Y (a), Nd^{3+} singly exchanged zeolite Y (b), and Nd^{3+}, Ag^+ ion-exchanged zeolite Y (c) individual particles treated at 900°C [17] (reproduced from American Institute of Physics).

As mentioned in Section 2.1.1, toward efficient emission from the RE or Bi ion-activated nanoporous zeolites, reducing or removing the hydrated water molecules is the key point. We found that co-loading Ag^+ ions into the cavities of zeolite Y can help collapse zeolite Y's structure; see **Figure 1**. Partial vitrification of the Nd^{3+} ion-exchanged zeolite Y was achieved at 900°C without extra crystalline phase introduction at the meantime. Partial elimination of water molecules can be identified from the FTIR spectra, where the absorption intensity due to the vibration of water molecules and hydroxyls both decreased for the partial vitrified sample, as shown in **Figure 2** (left). Due to the nonreversible dehydration in the vitrified parts of the partially collapsed Nd^{3+} ion-exchanged zeolite Y microcrystals, a six-fold enhancement of the 1053 nm NIR emission was achieved, as shown in **Figure 2** (right).

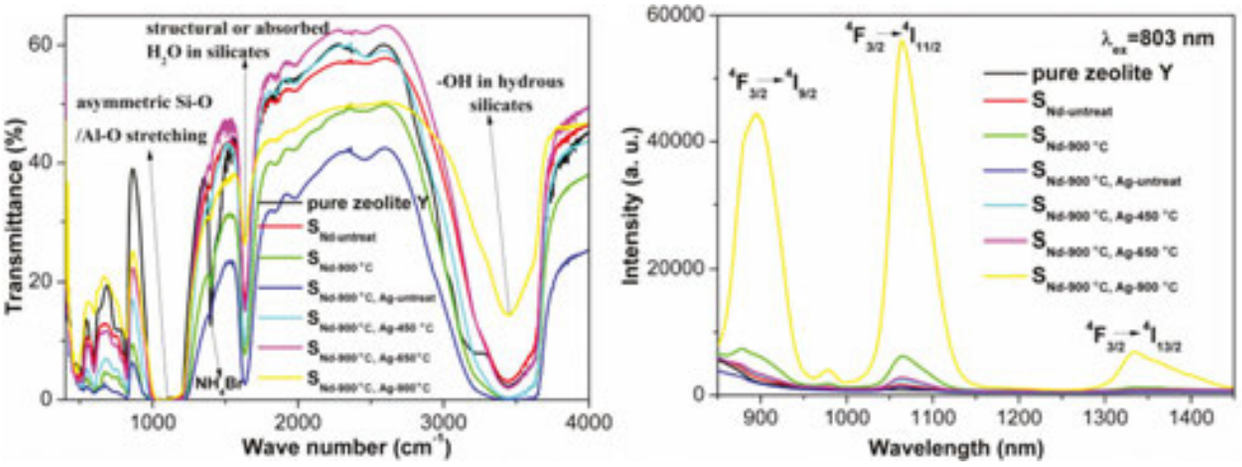

Figure 2. Left, FTIR spectra for the pure zeolite Y, Nd^{3+} ion-exchanged zeolite Y, and Nd^{3+}, Ag^{+} ion-exchanged zeolite Y under different thermal treatment conditions; right, NIR emission spectra of the Nd^{3+} (and Ag^{+}) ion-exchanged zeolite Y samples under different thermal treatment conditions [17] (reproduced from American Institute of Physics).

2.3. Up-conversion emission

Generally, there are few reports on the up-conversion (UC) emission from the RE ion-exchanged zeolites. This is probably due to the detrimental influence from hydrated water in the cavities, which can further decrease the low quantum efficiency of the up-conversion emission (usually less than 2%). Still, efforts have been devoted to this field, via extra coupling of molecules or radicals of low vibrational quanta, such as F^{-} and WO_4^{2-} [18], or partial dehydration by thermal treatment, or complete dehydration via collapsing the crystalline zeolite structure into glass-phase derivatives [19].

By employing the same method and taking advantage of blockade against water molecules by bismuth aggregates, that is, co-loading of bismuth ions into the zeolite Y's cavities combined with post-thermal treatment at 900°C, up-conversion green and red emissions have been achieved for the Er^{3+}, Yb^{3+}, and Bi^{3+} ions co-loaded zeolite Y powders [20].

2.4. Bismuth ion-exchanged zeolites for broad NIR emissions

2.4.1. Significance of the broad NIR emission from bismuth-activated materials

Since the first demonstration of broad NIR emission from bismuth-doped silica glass by Y. Fujimoto in 2001, research on the bismuth-activated broad NIR emitters has been conducted in various host lattices, involving nanocrystals, glasses, single crystals, and fibers (including both glass and crystalline fibers). The broad NIR (and mid-IR) emission from bismuth-activated luminescent materials falls well in the fiber-optic communication bands and hence is very promising as an alternative to the present commercial erbium (Er^{3+})- or thulium (Tm^{3+})-doped fibers and the erbium-doped fiber amplifiers (EDFA) for fiber-optic communication.

2.4.2. Broad NIR luminescence from bismuth ion-exchanged FAU zeolites and exploration on the NIR luminescent bismuth species

Exploration on the specific luminescent bismuth species is essential to promote the practical application of bismuth-doped materials, though it is complicated and challenging due to the rich oxidation states of bismuth ions. On the bismuth ion-exchanged zeolites, Sun and coworkers have contributed a series of work to the efficient broad NIR emission and the exploration on the bismuth species for the broad NIR emissions [15, 21, 22]. FAU zeolites, especially the Y-type possessing high-temperature structural duration due to the high Si/Al ratio, which is in favor of the dehydration process via relatively high-temperature thermal treatment, are chosen as the typical matrix for bismuth ions. Meantime, some by-product generated during the thermal treatment process may act as blockades for the Re-entry of water molecules. For instance, bismuth aggregates were proposed to be formed during the thermal annealing at 950°C and can prevent the water molecules from Re-entering the sodalite cages of zeolite Y; hence, strong NIR emission was achieved for the bismuth ion-exchanged zeolite Y powders, as depicted in **Figure 3**.

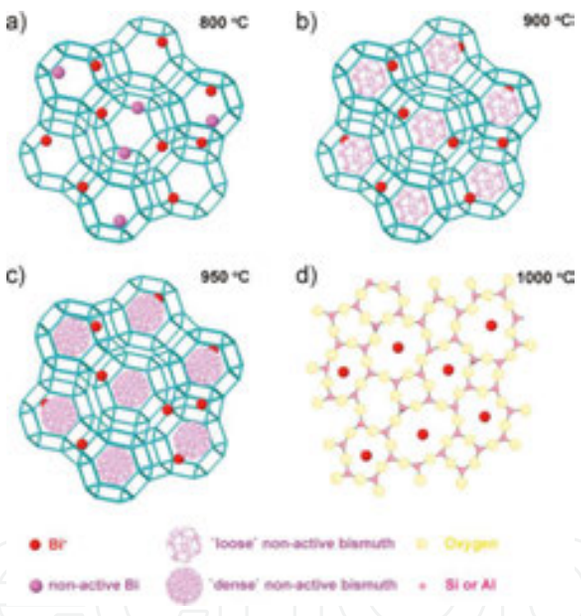

Figure 3. (a–c) Schematic illustration of the structure transformation of the zeolites annealed at different temperatures. (d) 2D representation of the structure of an aluminosilicate network. Note that "loose" and "dense" just represent small and large possibilities of sealing the pores of the zeolites with Bismuth agglomerates [15] (reproduced from John Wiley and Sons).

By high-resolution synchrotron X-ray diffraction (HR-XRD) (see **Figure 4**), photoluminescence (PL) spectra, electron spin resonance (ESR), nuclear magnetic resonance (NMR), and quantum chemistry calculation based on the spin-restricted relativistic time-dependent density functional theory (TDDFT), the broad emissions are assigned to several types of Bi^{+} substructures in the sodalite cages of zeolite Y. Bi^{+}, Bi_2^{2+}, Bi_3^{3+}, and Bi_4^{4+} are proposed to be the active luminescence centers in the sodalite cages of zeolite Y. Specifically, NIR emissions at 1050 nm,

1135 nm, 1145 nm, and 1240/1285 nm are assigned to Bi^{+}, Bi_2^{2+}, Bi_3^{3+}, and Bi_4^{4+}, respectively (**Figure 5**).

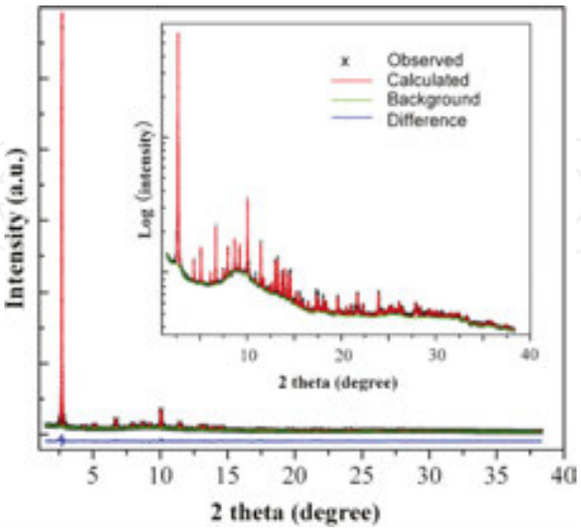

Figure 4. Rietveld fit to the high-resolution synchrotron XRD pattern of dehydrated Bi-embedded zeolite Y. Plots show the observed and calculated powder patterns. A difference curve is shown at the bottom of the diagram. Inset: a logarithmic-scale version of the graph [21] (reproduced from American Chemical Society).

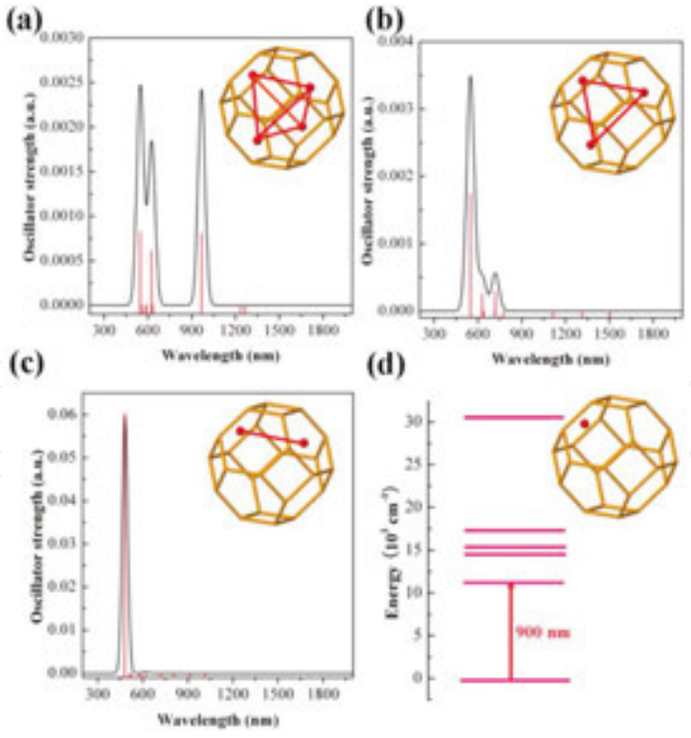

Figure 5. Theoretical absorption spectra for Bi_4^{4+} (a), Bi_3^{3+} (b), and Bi_2^{2+} (c). The energy-level diagram of Bi^{+} (d) was drawn according to the experimental absorption spectrum of $AlCl_3$-NaCl molten salt containing Bi^{+} [21] (reproduced from American Chemical Society).

2.5. Potential applications of the down- and up-conversion emission from RE and Bi ion-exchanged zeolites

Sun et al. demonstrated the bio-imaging in the second biological window with the amorphous aluminosilicate nanoparticles derived from FAU and LTA zeolites nanocrystals. The FAU and LTA zeolite nanocrystals are synthesized by the hydrothermal growth [23]. Bismuth ions were incorporated into the zeolite FAU and LTA nanocrystals' cavities via ion exchange and then subjected to thermal treatment at 870°C for 15 min, after which amorphous Bi ion-doped aluminosilicate nanoparticles were obtained. Finally, a 22 nm-thick silica layer was coated on the surface of Bi ion-doped aluminosilicate amorphous nanoparticles to improve the biocompatibility. In vivo bio-imaging in the second biological window (1–1.35 μm) for a mouse was successfully demonstrated by employing the silica-coated Bi ion-doped aluminosilicate nanoparticles derived from FAU and LTA zeolite nanocrystals.

Two main features of this material for in vivo bio-imaging applications are the relatively long emission decay time (hundreds of microseconds), which is in favor of the fluorescence lifetime imaging microscopy, and the emission wavelength in the second biological window, which provides higher spatial resolution than that of bio-imaging based on fluorescence in the first biological window (0.65–0.95 μm) [24].

Besides bio-imaging, down-conversion NIR emission from RE and Bi ion-exchanged zeolites which can split one UV-vis photon into two or more NIR photons may also have application as the converter layer to improve the conversion efficiency of crystalline silicon solar cells.

2.6. Possible future work

So far, average sizes of most commercial available zeolite powder matrices are in the range of micrometer or sub-micrometer scales; for instance, the typical edge length of the LTA zeolite cube (micro-single crystal) is about 1–2 μm. This size is too large for bio-imaging applications. Nanoporous zeolite nanocrystals with the average size from tens of, to several hundred nanometers, may be possible to get dispersed in water to facilitate the bio-applications.

Further detailed structure characterization of the RE and Bi ion-exchanged and thermal-treated zeolite micro-/nanocrystals is worth conducting, since the luminescent active centers incorporated in the glass-phase parts may also contribute to the emission.

It is worth trying whether it is possible to observe up-conversion emission color tuning via adsorption/de-adsorption of molecules, for example, small polar molecules such as H_2O, H_2S, and NH_3 or small organic molecules. Tuning of the UC emission color is expected to be enabled by the overall phonon energy change of the whole host-guest system upon adsorption/de-adsorption of different guest molecules of different phonon energies.

http://dx.doi.org/10.5772/63805

3. d^{10} ion-exchanged zeolites

3.1. One question about the reversible color change of Ag^+ ion-exchanged LTA zeolites

The reversible color change of Ag^+ ion-exchanged LTA was reported by Rálek et al. [25]. This color change was generally attributed to formation of Ag_m^{n+} clusters [26]. Till 1998, this phenomenon was explained in the way of charge transfer transition from the framework oxygen to the empty 5s orbit of the extra-framework Ag^+ ions [27]. This reversible color change can be achieved under very low Ag^+ ion loading concentration (Ag^+-Na^+ exchanging ratio equals 1/96) and dehydration at room temperature in vacuum without thermal treatment, in which condition, in principle Ag clusters were almost impossible to be formed due to the considerably light loading of Ag^+ ions. Interestingly, except for the assignment of the reversible color change, most of the later work on luminescence from the Ag^+ ion-exchanged zeolites still assigned the few-atom silver clusters [28–30], such as Ag_3^+ and Ag_6^+ to the luminescence origin other than the charge transfer transition [31, 32].

3.2. Methods to activate the Ag^+ ion-exchanged nanoporous luminescent zeolites

So far, various methods have been tried to activate the luminescence from the Ag^+ ion-exchanged nanoporous zeolites, such as UV laser illumination, X-ray irradiation, and the most often adopted thermal treatment. The role of UV laser in activating the visible emission can be observed by sharp contrast for one piece of Ag^+ ion-exchanged micro-crystal through comparing the regions with/without light irradiation. The mechanism of activation by UV illumination [33] and X-ray irradiation [34] was explained in the way of photo-reduction of Ag^+ into Ag^0 atoms and then the formation of Ag_n^{m+} clusters. It should be pointed out that besides the explanation from the view of formation of Ag_n^{m+} clusters, dehydration by the heat effect under the irradiation of high energy light beam may also contribute to the luminescence activation.

3.3. Reversible emission variation of Ag^+ ion-exchanged LTA and SOD zeolites and possible mechanisms for this process

It should be noted that the terminology "cluster" is widely adopted among different communities for different types of metal nanospecies. For instance, for metal-organic complexes, aggregates of metal ions in close contact via the weak metallophilic interaction are also called clusters (short for cluster A hereinafter). During the past two decades, few-atom, sub-nm scale (below 1 or 2 nm) noble and coinage (Au, Ag, Pt, Pd, and Cu) metal nanospecies bonded via the metal-metal bonds as the same as in bulk metals or molecular-like bonds are also called clusters (short for cluster B hereinafter).

So far, the origin of emission from cluster B is still not sufficiently clear. At present, explanations from the following two ways have been mainly proposed: one is based on the free electron theory combined with quantum confinement effect; the other is based on the super atom theory. To explore the emission mechanisms of the metal clusters, first the interaction type

between the neighboring metal ions or atoms needs to be clarified. It is a pity that this issue did not seem to be clearly addressed in lots of the previous work.

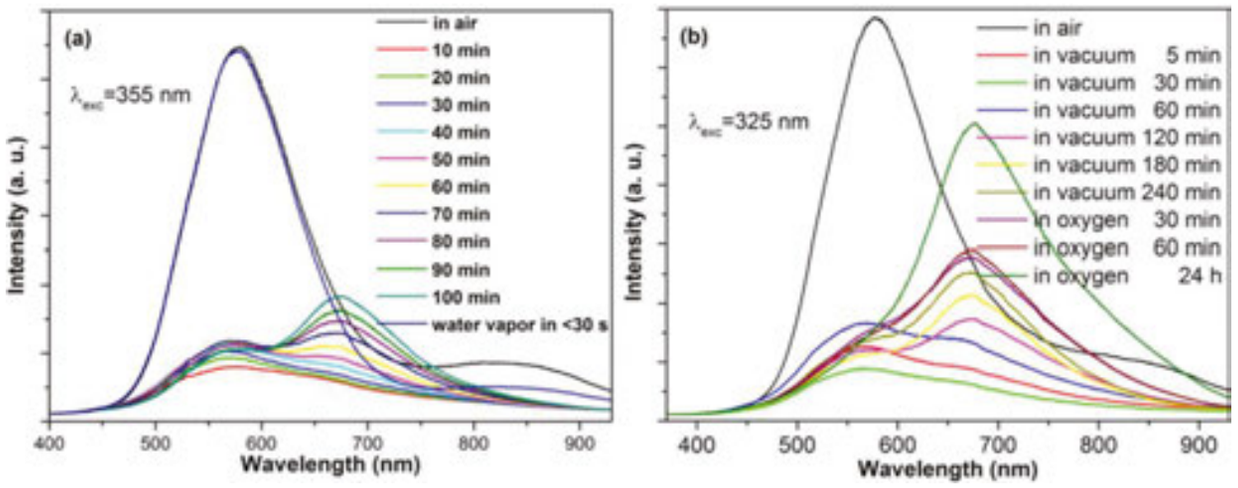

Figure 6. PL evolution of $Ag_{4.4}$, $Na_{7.6}$-A from air to vacuum then to water vapor (a) or oxygen (b) [35] (reproduced from American Institute of Physics).

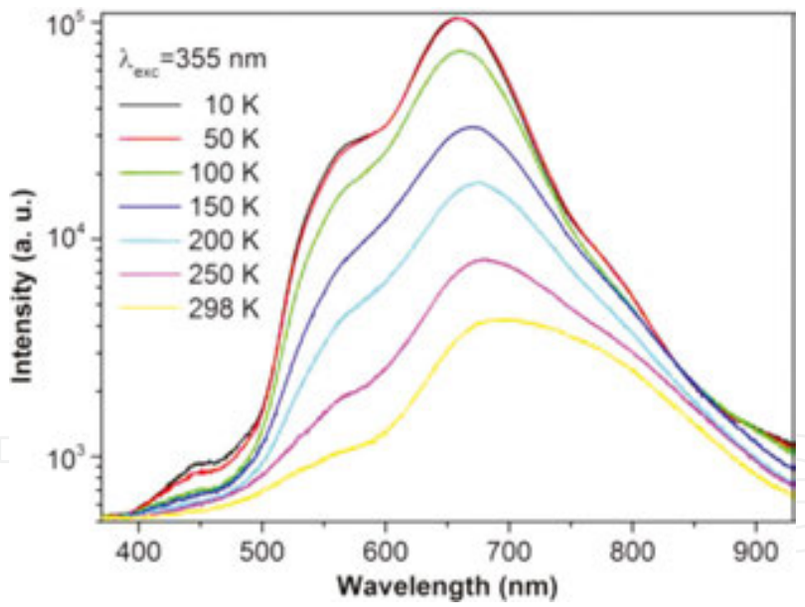

Figure 7. Temperature-dependent PL spectra for $Ag_{4.4}$, $Na_{7.6}$-A under the 355 nm excitation [35] (reproduced from American Institute of Physics).

Recently, H_2O molecule-sensitive, reversible green/red-dominant emission evolution was observed for the Ag^+ ion-exchanged LTA zeolite (see **Figure 6**), and different from most of the previous reports, the yellow-green emission is not assigned to Ag_n^{m+} cluster [35]. Confirmation of the role of H_2O molecules in the reversible emission evolution was achieved with the assistance of a designed vacuum chamber, into which different gas species such as N_2, O_2, and

H_2O vapor can be introduced. The reversible emission evolution process observed from the Ag^+ ion-exchanged LTA zeolites upon desorption/adsorption of H_2O molecules led us to reflect that the interaction between the neighboring Ag^+-Ag^+ ions does not seem to be the metal bonds while it may be the weak argentophilic (Ag^+---Ag^+) interaction.

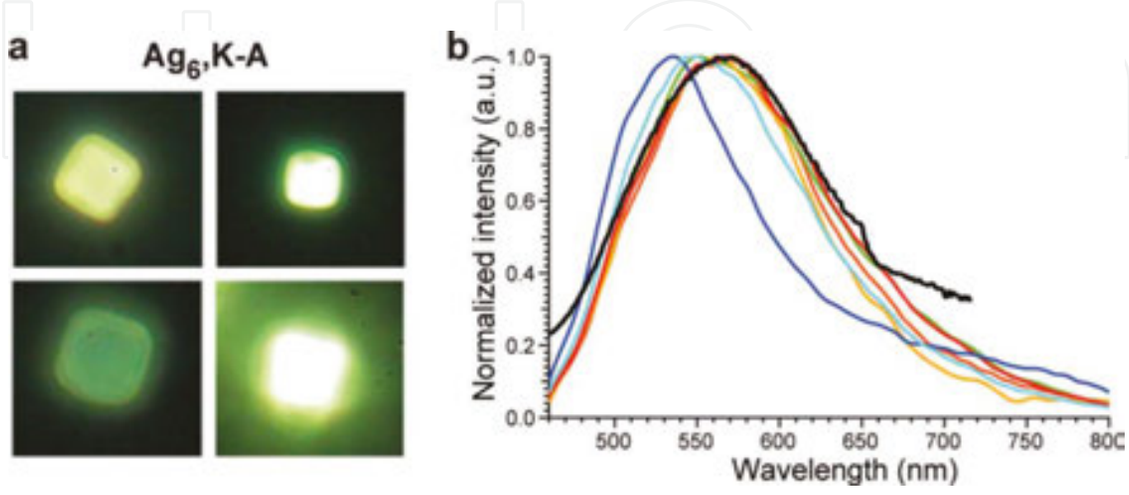

Figure 8. Single-crystal emission characterization for the Ag_3^+ clusters inside zeolite A upon UV excitation. (a) The individual crystals have sizes ranging from 2 to 5 μm. (b) Emission spectra of Ag_6Na-A zeolites upon 400-nm illumination. The black curve corresponds to the bulk spectrum (measured in a fluorimeter), while the colored curves represent spectra from individual crystals measured on a confocal fluorescence microscope [28] (reproduced from the American Chemical Society).

There is no obvious narrowing of the emission band in the PL spectra of the Ag^+ ion-exchanged LTA zeolites taken at cryogenic temperature as low as 10 K (**Figure 7**). Pioneering work on comparing the PL spectra of the Ag^+ ion-exchanged LTA zeolite micro-crystals' ensemble and individual micro-crystals proves that there is no obvious inhomogeneous broadening contributing to the broad emission, as shown in **Figure 8**.

The H_2O molecule-sensitive, reversible emission evolution and the broad emission band at 10 K, together with the negligible contribution from inhomogeneous broadening, suggest that the emission from the Ag^+ ions containing LTA zeolites is not attributed to the quantum confinement effect. Corresponding to the origin of the reversible color change of Ag^+ ion-exchanged LTA zeolites upon dehydration/hydration, the green emission can be assigned to the framework $O^{2-} \rightarrow Ag^+$ (coordinated by water) ligand to metal charge transfer (LMCT) transition. Since there are two sets of cages (α-cages and β-cages) in LTA zeolites, it is difficult to propose further detailed physical scenario for the H_2O molecule-sensitive reversible green/red dominant emission evolution. So SOD zeolite, which consists of the sodalite cages and has very similar chemical composition to LTA zeolite, was employed as the matrix for Ag^+ ions, in hope to provide more specific information about the H_2O molecule-sensitive emission phenomenon.

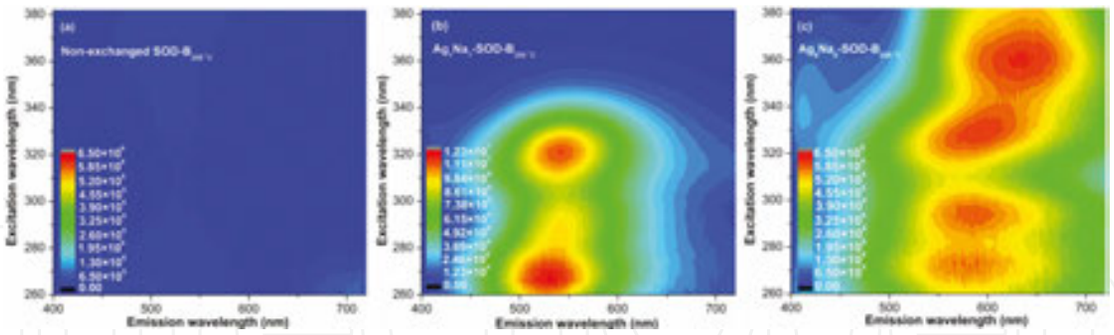

Figure 9. Excitation-emission 3D contours of non-exchanged SOD-$B_{250°C}$ (a), Ag_1Na_7-SOD-$B_{250°C}$ (b), and Ag_8Na_0-SOD-$B_{250°C}$ (c) [36] (reproduced from Royal Society of Chemistry).

The PL characteristics of the Ag^+ ion-exchanged SOD zeolites with different Ag^+ loading concentrations are similar to the Ag^+ ion-exchanged LTA counterparts. That is, under low Ag^+ loading concentration, only green emission can be observed, while under high Ag^+ loading concentration, red emission can be observed, as shown in **Figure 9**. Though not being as obvious as the situation for the Ag^+ ion-exchanged LTA zeolites, similar H_2O molecule-sensitive, reversible emission variation of the Ag^+ ion-exchanged SOD zeolites in vacuum/air or water vapor environment was observed [36], as shown in **Figure 10**.

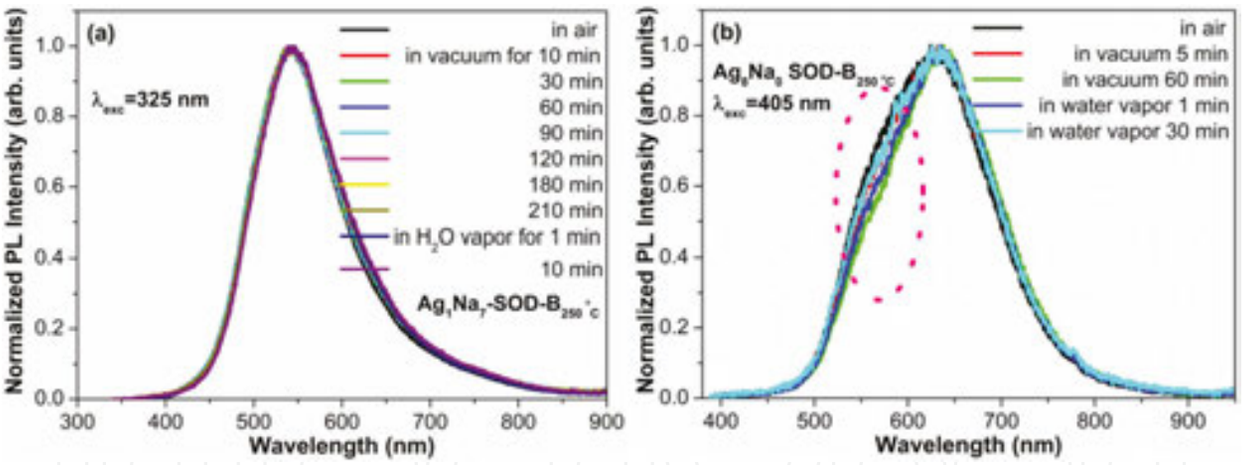

Figure 10. PL spectra recorded in different environmental conditions for Ag_1Na_7-SOD-$B_{250°C}$ (a) and Ag_8Na_0-SOD-$B_{250°C}$ (b) [38] (reproduced from Royal Society of Chemistry).

The low-lying excited states of Ag^+ ions (aggregates) enabling the visible or even NIR emission are commonly seen in the Ag(I)-organic complexes. In contrast, this phenomenon is rare for inorganic materials. So far, several types of inorganic materials have been reported with this kind of capability, such as the Ag^+-doped (or containing) oxyfluoride glasses, $K[Ag(I)CN_2]$ [37], or simply the Ag^+ ion-exchanged LTA and SOD zeolites. Note that for the Ag^+ ion-exchanged zeolites, it is shown that the amount of negative charges in zeolites' framework seems to have a key role in tuning down the emission energy, since sharp contrast has been observed between the emission energy of Ag^+ ion-exchanged LTA (or SOD) and Ag^+ ion-exchanged ZSM-5

zeolites. Specifically, green or red visible emissions can be observed from the Ag^+ ion-exchanged LTA (or SOD) zeolites (Al/Si ratio = 1), while only emissions in the UV region were observed from the Ag^+ ion-exchanged ZSM-5 zeolites (Al/Si ratio = 11.65). This is in good accordance with conclusions that the high-lying excited state of Ag^+ can be modified via ligand to metal or metal to metal charge transfer transition, especially when a reducing ligand is present [38].

With the complementary information obtained from the Ag^+ ion-exchanged SOD zeolites, a specific physical scenario for the H_2O molecule-sensitive reversible emission variation is proposed: the yellow-green emission is due to the ligand to metal (framework $O^{2-} \rightarrow Ag^+$) charge transfer transition within the partial hydration state, and the red emission is attributed to the ligand to metal-metal (framework $O^{2-} \rightarrow Ag^+$-Ag^+) or metal-metal (Ag^+-Ag^+) charge transfer transition upon dehydration when the water molecules which block the interaction between the neighboring Ag^+ ions are removed (see **Figure 11**).

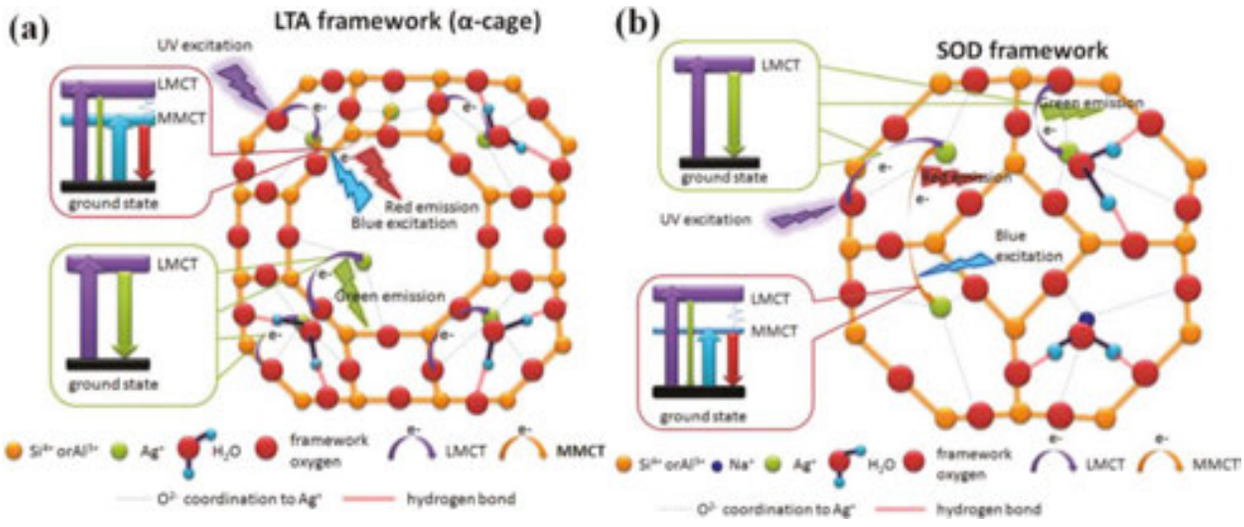

Figure 11. Proposed emission mechanisms in Ag^+ ion-exchanged LTA (a) and SOD (b) zeolites [36] (reproduced from Royal Society of Chemistry).

Though the emission variation tendency for the Ag^+ ion-exchanged SOD zeolites is similar to that of the Ag^+ ion-exchanged LTA zeolites, the recovery time for the emission variation from vacuum to H_2O vapor is much slower (~30 min) than the counterpart of Ag^+ ion-exchanged LTA zeolites (≤30 s). This can be attributed to the slow diffusion of H_2O molecules in SOD zeolites consisting of only the β-cages without straight, large channels (critical size 2.53 Å). In LTA, H_2O molecules can fast permeate along the 3D channels with the critical size of 4.21 Å confined by the 8-rings of the α-cage.

Location preference of the Ag^+ ions and Ag_n^{m+} clusters in LTA zeolite (either in the α-cage or the β-cage) is still controversial [39, 40]. From the contrasting response time of emission variation between the Ag^+ ion-exchanged LTA and SOD zeolites, it is suggested that for LTA zeolite Ag^+ ions are mainly located in the α-cage.

3.4. Potential optical and photonic applications of the Ag^+ ion-exchanged nanoporous zeolites

So far, by employing Ag^+ ion-exchanged nanoporous zeolites, promising optical and photonic applications have been demonstrated, such as optical recording and LED phosphors. Besides, the emission color change accompanied with reversible adsorption/de-adsorption of H_2O may have application as photoluminescence responsive sensors for small polar molecules or molecular tweezers.

Author details

Hui Lin and Minoru Fujii*

*Address all correspondence to: fujii@eedept.kobe-u.ac.jp

Department of Electrical and Electronic Engineering, Graduate School of Engineering, Kobe University, Kobe, Japan

References

[1] H. Lim, S.-E. Choi, H. Cheong, and J. S. Lee, *Micropor. Mesopor. Mater*., 2014, 192, 89-94.

[2] L. Gartzia-Rivero, J. Banelos-Prieto, V. Martinez-Martinez, and I. Lopez Arbeloa, *ChemPlusChem*, 2012, 77, 61-70.

[3] M. Xue, L. Fan, Z. Kang, W. Zhang, H. Li, and S. Qiu, *J. Mater. Chem*., 2012, 22, 17644-17648.

[4] N. S. Kehr, J. El-Gindi, H.-J. Gallab, and L. D. Cola, *Micropor. Mesopor. Mater*., 2011, 144, 9-14.

[5] I. Lopez-Duarte, L.-Q. Dieu, I. Dolamic, M. V. Martinez-Diaz, T. Torres, G. Calzaferri, and D. Brühwiler, *Chem. Eur. J*., 2011, 17, 1855-1862.

[6] K. Y. Yoon, *Acc. Chem. Res*., 2007, 40, 29-40.

[7] S. Fibikar, G. Luppi, V. Martinez-Junza, M. Clemente-Leon, and L. D. Cola, *ChemPlusChem*, 2014, 79, 1-6.

[8] F. Cucinotta, Z. Popovic, E. A. Weiss, G. M. Whitesides, and L. D. Cola, *Adv. Mater*., 2009, 21, 1142-1145.

[9] S. Fibikar, G. Luppi, V. Martínez-Junza, M. Clemente-León, and L. D. Cola, *ChemPlusChem*, 2015, 80(1), 62-67.

[10] G. Calzaferria, H. Maas, M. Pauchard, M. Pfenniger, S. Megelski, and A. Devaux, *Adv. Photochem*., 2002, 27, 1-50.

[11] A. Devaux, G. Calzaferri, P. Belser, P. Cao, D. Brühwiler, and A. Kunzmann, *Chem. Mater*., 2014, 26, 6878-6885.

[12] C. Leiggener and G. Calzaferri, *Chem. Eur. J*., 2005, 11, 7191-7198.

[13] X. Mao, S. Wang, S. Shimai, and J. Guo, *J. Am. Ceram. Soc*., 2008, 91(10), 3431-3433.

[14] J. Akiyama, Y. Sato, and T. Taira, *Opt. Lett*., 2010, 35(21), 3598-3600.

[15] H.-T. Sun, A. Hosokawa, Y. Miwa, F. Shimaoka, M. Fujii, M. Mizuhata, S. Hayashi, and S. Deki, *Adv. Mater*., 2009, 21, 3694-3698.

[16] Y. Wada, T. Okubo, M. Ryo, T. Nakazawa, Y. Hasegawa, and S. Yanagida, *J. Am. Chem. Soc*., 2000, 122, 8583-8584.

[17] H. Lin, S. Rong Gui, K. Imakita, and M. Fujii, *J. Appl. Phys*., 2014, 115, 033507.

[18] M. M. Lezhnina, and U. H. Kynast, *Phys. Sol. State*, 2005, 47, 1485-1488.

[19] Y. Gong, H. Chen, Q. He, J. Shi, L. Wang, W. Jiang, *Ceram. Int*., 2013, 39, 8865-8868.

[20] Z. Bai, M. Fujii, K. Imakita, and S. Hayashi, *Micropor. Mesopor. Mater*., 2013, 173, 43-46.

[21] H.-T. Sun, Y. Matsushita, Y. Sakka, N. Shirahata, M. Tanaka, Y. Katsuya, H. Gao, and K. Kobayashi, *J. Am. Chem. Soc*., 2012, 134, 2918-2921.

[22] H.-T. Sun, Y. Sakka, N. Shirahata, Y. Matsushita, K. Deguchi, and T. Shimizu, *J. Phys. Chem. C*, 2013, 117, 6399-6408.

[23] H.-T. Sun, J. Yang, M. Fujii, Y. Sakka, Y. Zhu, T. Asahara, N. Shirahata, M. Ii, Z. Bai, J. Li, and H. Gao, *Small*, 2011, 7, 199-203.

[24] G. Hong, J. C. Lee, J. T. Robinson, U. Raaz, L. Xie, N. F. Huang, J. P. Cooke, and H. Dai, *Nat. Med*., 18(12), 1841-1848 (2012).

[25] M. Rálek, P. Jírů, O. Grubner, and H. Beyer, *Collect. Czech. Chem. Commun*., 1962, 27, 142.

[26] L. R. Gellens, W. J. Mortier, R. A. Schoonheydt, and J. B. Uytterhoeven, *J. Phys. Chem*., 1981, 85, 2783.

[27] R. Seifert, A. Kunzmann, and G. Calzaferri, *Angew. Chem. Int. Ed*., 1998, 37, 1521.

[28] G. D. Cremer, E. Coutiño-Gonzalez, M. B. J. Roeffaers, B. Moens, J. Ollevier, M. V. der Auweraer, R. Schoonheydt, P. A. Jacobs, F. C. De Schryver, J. Hofkens, D. E. De Vos, B. F. Sels, and T. Vosch, *J. Am. Chem. Soc*., 2009, 131, 3049.

[29] H. Lin, K. Imakita, S.C.R. Gui, and M. Fujii, *J. Appl. Phys*., 2014, 116, 013509.

[30] H. Hoshino, Y. Sannohe, Y. Suzuki, T. Azuhata, T. Miyanaga, K. Yaginuma, M. Itoh, T. Shigeno, Y. Osawa, and Y. Kimura, *J. Phys. Soc. Jpn*., 2008, 77, 064712.

[31] G. Calzaferri, C. Leiggener, S. Glaus, D. Schürch, and K. Kuge, *Chem. Soc. Rev*., 2003, 32, 29.

[32] R. Seifert, R. Rytz, and G. Calzaferri, *J. Phys. Chem. A*, 2000, 104, 7473.

[33] G. D. Cremer, Y. Antoku, M. B. J. Roeffaers, M. Sliwa, J. V. Noyen, S. Smout, J. Hofkens, D. E. De Vos, B. F. Sels, and T. Vosch, *Angew. Chem. Int. Ed*., 2008, 47, 2813.

[34] E. Coutino-Gonzalez, D. Grandjean, M. Roeffaers, K. Kvashnina, E. Fron, B. Dieu, G. D. Cremer, P. Lievens, B. Sels, and J. Hofkens, *Chem. Commun*., 2014, 50, 1350.

[35] H. Lin, K. Imakita, and M. Fujii, *Appl. Phys. Lett*., 2014, 105, 211903.

[36] H. Lin, K. Imakita, M. Fujii, V. Y. Prokof'ev, N. E. Gordina, B. Saïdc, and A. Galarneau, *Nanoscale*, 2015, 7, 15665-15671.

[37] M. A. Rawashdeh-Omary, M. A. Omary, H. H. Patterson, and J. P. Fackler, Jr., *J. Am. Chem. Soc*., 2001, 123(45), 11237-11247.

[38] F. Sabin, C. K. Ryu, P. C. Ford, and A. Vogler, *Inorg. Chem*., 1992, 31(10), 1941-1945.

[39] R. Seifert, R. Rytz, and G. Calzaferri, *J. Phys. Chem. A*, 2000, 104, 7473.

[40] T. Sun and K. Seff, *Chem. Rev*., 1994, 94, 857.